Electronic Supplementary Material (ESI) for Materials Advances.
This journal is © The Royal Society of Chemistry 2021

Supporting information

Design of $Co_1Al_3(OH)_m$/Carbon Nitride hybrid Nanostructure for Enhanced Capacitive Energy Storage in Alkaline Electrolyte

Prajnashree Panda, Ranjit Mishra, Sonali Panigrahy, Sudip Barman*

School of Chemical Sciences, National Institute of Science Education and Research (NISER), HBNI, Bhubaneswar, PO Bhimpur-Padanpur, Via Jatni, District Khurda, Orissa - 752050, India.

E-mail: sbarman@niser.ac.in. Tel: +91(674)2494183.

Characterizations:

The x-ray diffraction data (p-XRD) of as prepared samples were conducted by Bucker DAVINCI D8 ADVANCE diffractometer equipped with a monochromatic radiation source of Cu kα (λ= 0.15406).The composition and morphology of the material was recorded by Field-emission scanning electron microscope (FESEM) system (Carl Zeiss, Germany make, Model: ∑igma) and Transmission Electron Microscopy (TEM,JEOL F200) and High-Resolution TEM (HRTEM).VG Microtech was used to record the XPS data with monochromatic Mg K_α X-ray as the source. IR data was collected by using Perkin Elmer RXI FT-IR spectrophotometer. All electrochemical measurements were performed by using CorrTest Electrochemical Workstation [Model: CS350]. Quantachrome Instruments (AutosorbiQ-XR-XR (2 Stat.)) Viton was used to determine the Specific surface area by N_2 adsorption-desorption isotherm**.** ICP-OES data was collected on iCAP 7000 Series (Thermo Scientific). Before experiment, pH of the working solution was measured by Hanna (HI 2209) pH meter.

Electrochemical measurements:

Cyclic voltammetry (CV), galvanostatic charging-discharging (GCD) tests and EIS were performed by using Corr Test Electrochemical Workstation [Model: CS350]. EIS measurements were conducted in the frequency range of 0.1 to 100 kHz with 5 mV AC amplitude under open circuit potential. All electrochemical measurements were performed in 2M KOH aqueous solution at room temperature. For half-cell configuration platinum wire , Ag/AgCl and active material coated on 1×1 cm^2 Ni foam were used as counter, reference and working electrode respectively. Cyclic voltammetry curves were recorded in a potential range of 0-0.55V at scan rate ranging from 5-100 mV/sec.

Specific capacitance of the as synthesized material was calculated by using eq^n (1)[1, 2]

$$C_s = \frac{I\Delta t}{m\Delta V} \quad (1)$$

$$\Delta V \times C_s = \frac{I\Delta t}{m} = Q \quad (1(a))$$

Specific capacitance (C_s) can be calculated from the CV curve by using the eq^n (2)

$$C_s = \frac{\int IdV}{2m\Delta V \upsilon} \quad (2)$$

Where C_s is the specific capacitance (F/g), Q is the specific capacitance (mAh/g) I is the current applied (mA), Δt is the discharge time (sec), m is the mass of active material (mg), ΔV is the operating potential window (V), $\int Idv$ is the area under the CV curve and υ denotes the scan rate (mV/s).

For Asymmetric supercapacitor (ASC) cell the as prepared material (active material) act as cathode and commercial AC act as anode. The full cell is represented as $Co_1Al_3(OH)_m/CN_x$//AC. In order to balance the charge storage the mass ratio of $Co_1Al_3(OH)_m/CN_x$ and AC was calculated by using eq^n (3)

$$\frac{m+}{m-} = \frac{C+\Delta V+}{C-\Delta V-} \quad (3)$$

Where m_+ was the mass (mg), C_+ and C_- were the specific capacitance of active material and AC respectively, ΔV_+ and ΔV_- is the voltage window of cathode and anode electrode respectively and m_- was the mass of anode.

$$E = \frac{Cs(\Delta V)2}{7.2} \quad (4)$$

$$P = \frac{E}{\Delta t} \times 3600 \quad (5)$$

Where ΔV is the voltage window (V), Cs is is the capacitance of ASC (F/g) and Δt is the discharge time (sec)

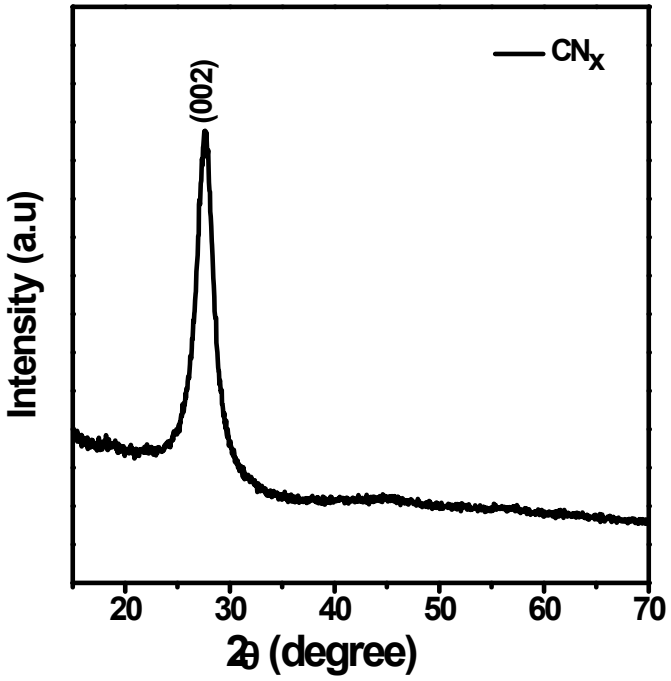

Figure S1. p-XRD pattern of CN_x

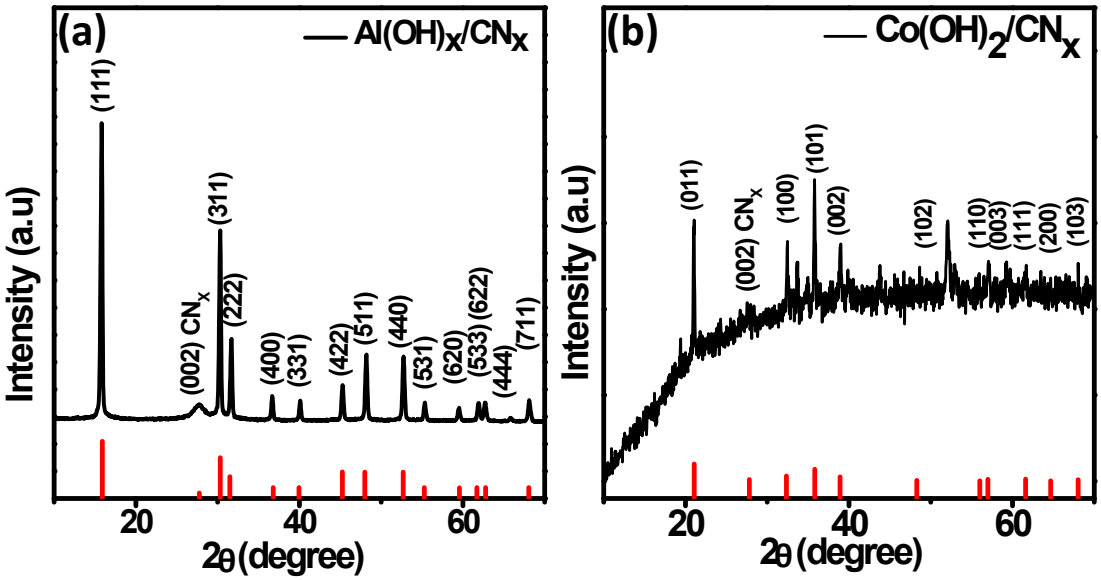

Figure S2. p-XRD pattern of (a) $Al(OH)_x/CN_x$ and (b) $Co(OH)_2/CN_x$ respectively

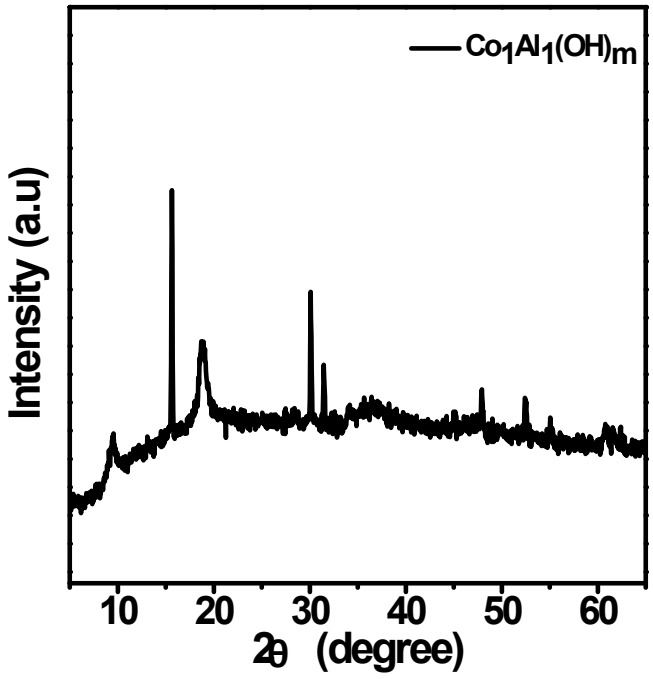

Figure S3. p-XRD pattern of $Co_1Al_3(OH)_m$

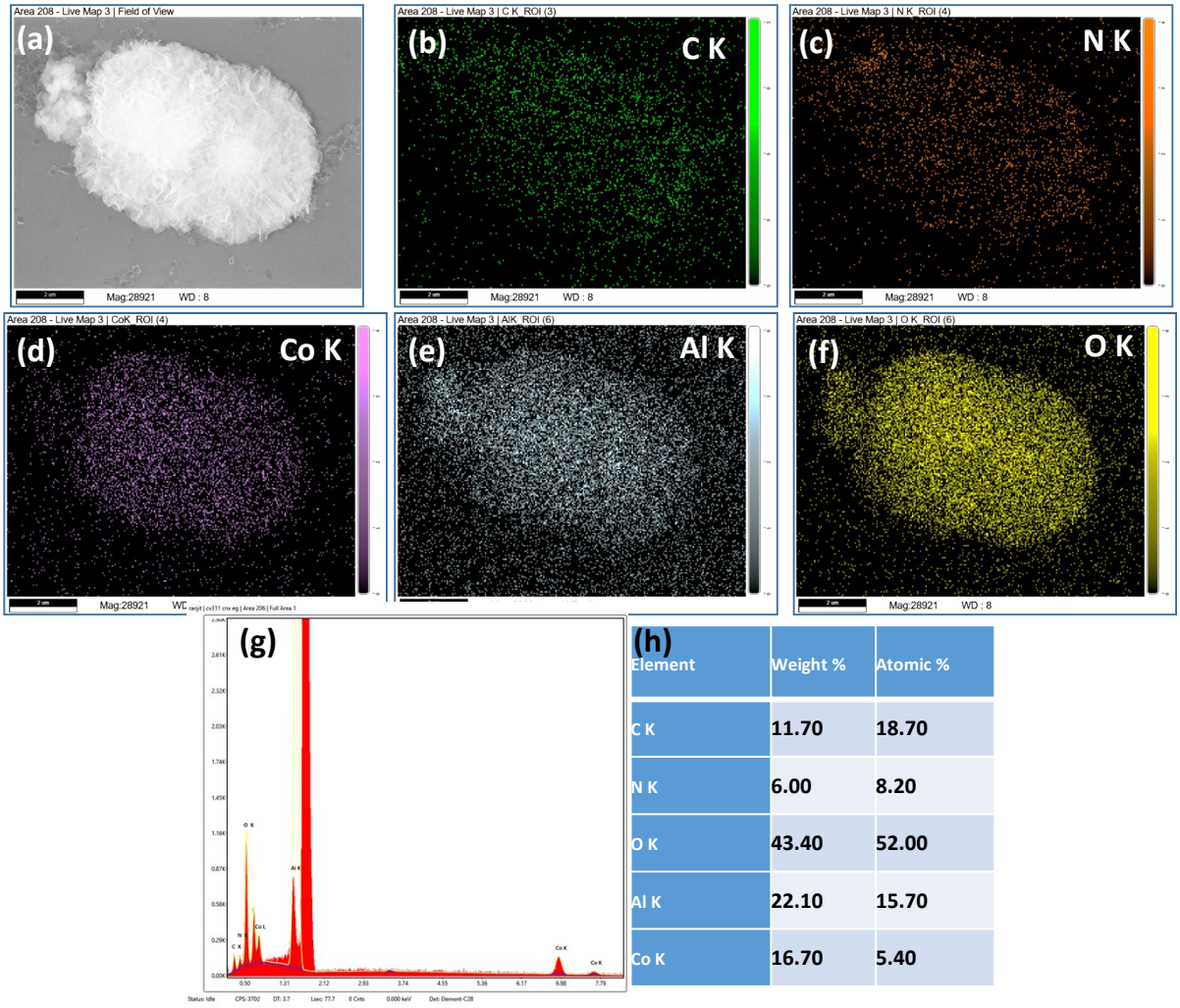

(h)

Element	Weight %	Atomic %
C K	11.70	18.70
N K	6.00	8.20
O K	43.40	52.00
Al K	22.10	15.70
Co K	16.70	5.40

Figure S4.(a) SEM image and corresponding Elemental mapping of elements (b) C (c) N (d) Co (e) Al (f) O of $Co_1Al_3(OH)_m/CN_x$ showing an uniform distribution of C, N, Co, Al and O (g) FESEM EDS profile and (h) weight percentage and atomic percentage of different elements.

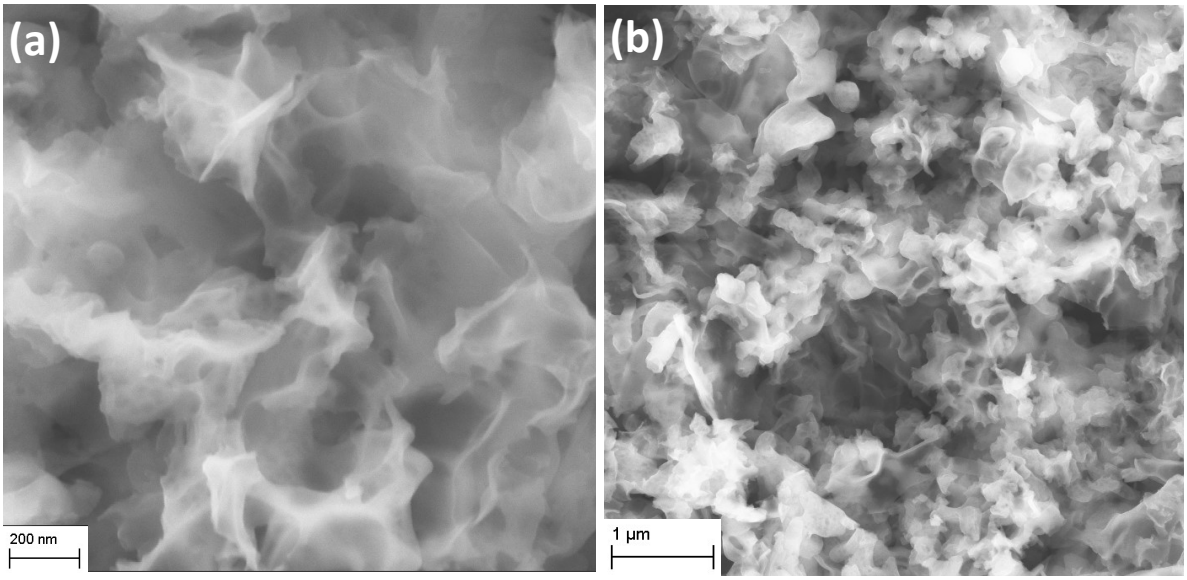

Figure S5. SEM image of CN_x

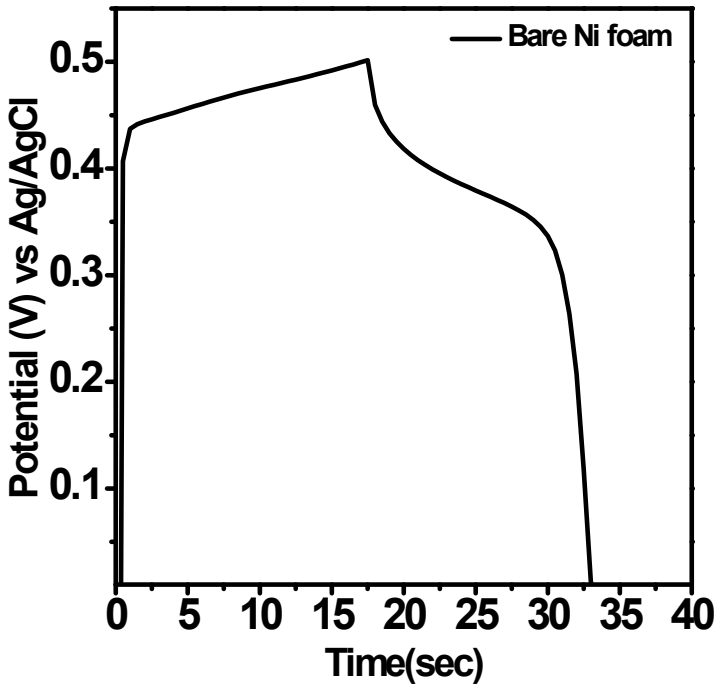

Figure S6. GCD curves of bare Ni foam at 1 A/g current density

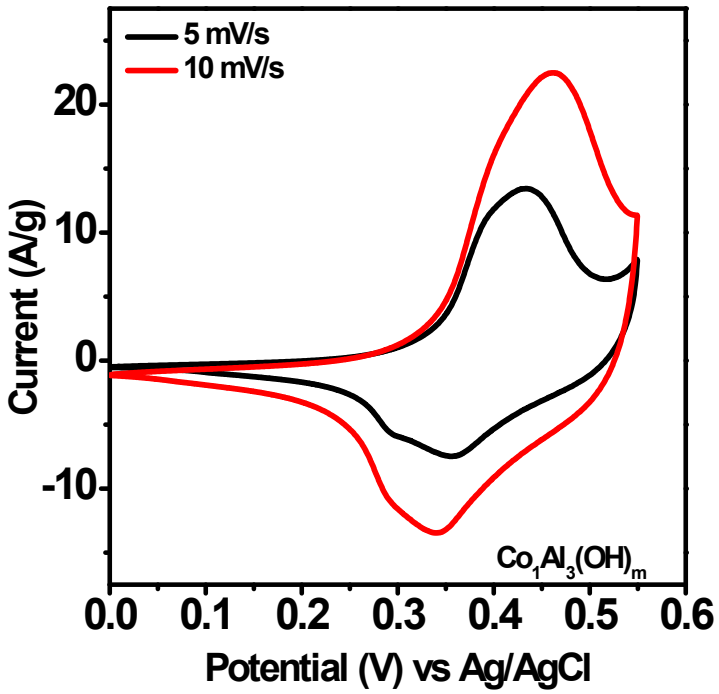

Figure S7. CV curves of $Co_1Al_3(OH)_3$ at diff. scan rate

Table S1. Composition analysis of the Co_1Al_δ $(OH)_m/CN_x$ (δ=1, 2, 3, 4) composites from elemental mapping

Composite	Amount of Co and Al (Atomic %) (EDS)	
	Co	Al
Co_1Al_1 $(OH)_m/CN_x$	4.3	3.6
Co_1Al_2 $(OH)_m/CN_x$	2.4	4.6
Co_1Al_3 $(OH)_m/CN_x$	5.4	15.7
Co_1Al_4 $(OH)_m/CN_x$	3.9	16.5

Table S2. Relative percentage of area and atomic ratio of Co^{+2}/Co^{+3} in Co $2p_{3/2}$ and $2p_{1/2}$ of $Co_1Al_3(OH)_m/CN_x$ composite

Peak	Relative area (%) of Co^{+2}	Relative area (%) of Co^{+3}	Co^{+2}/Co^{+3}
Co $2p_{3/2}$	679.5	349.4	1.95
Co $2p_{1/2}$	365	189.5	1.93

Table S3. Comparison of electrochemical performance of $Co_1Al_3(OH)_m/CN_x$ composite with previously reported literatures

Electrode material	Specific capacitance of single Electrode	Capacitance retention after cycling stability	No. of cycles	Ref.
CoAl-LDH/GF	101.4 F/g (0.5 A/g)	-	-	[3]
Co-Al LDH/GHA	640 F/g (1 A/g)	97	10000	[4]
Co-Al LDH/rGO-3	1492 F/g (1 A/g)	94.3	5000	[5]
g-C_3N_4 nanosheet@CoAl-LDH	343.3 F/g (5 A/g)	95.28	6000	[6]
CoAl LDHs-0.5	799.2 F/g (1 A/g)	82	5000	[7]
$Co_2Al(OH)_{7-2x}(CO_3)_x.nH_2O$	900 F/g (1 A/g)	100	1000	[8]
CoAl-S8	1150.6 F/g (1 A/g)	97.8	1000	[9]
CAN-LDH-NS-rGO	1296 F/g (1 A/g)	90.5	1000	[10]
Co-Al LDH-NS/GO	1031 F/g (1 A/g)	100	6000	[11]
CoAl LDH@PEDOT	672 F/g (1 A/g)	63.1	5000	[12]
CoS-20	365 F/g (10 A/g)	91.2	1300	[13]
Co_3O_4/CoO	362.8 F/g (0.2 A/g)	78.7	1000	[14]
NiFRS	198 C/g (1 A/g)	46	-	[15]
FeSC1	683.2 C/g (1 A/g)	-	-	[16]
$Co_1Al_3(OH)_m/CN_x$	1000 F/g (1 A/g)	84.46	4500	This work

References

[1] X. Zhai, J. Gao, X. Xu, W. Hong, H. Wang, F. Wu, Y. Liu, Journal of Power Sources 396 (2018) 648-658.
[2] K. Wang, B. Lv, Z. Wang, H. Wu, J. Xu, Q. Zhang, Dalton Transactions 49 (2020) 411-417.
[3] T.M. Masikhwa, M.J. Madito, D.Y. Momodu, J.K. Dangbegnon, O. Guellati, A. Harat, M. Guerioune, F. Barzegar, N. Manyala, RSC Advances 6 (2016) 46723-46732.
[4] A. Zhang, C. Wang, Q. Xu, H. Liu, Y. Wang, Y. Xia, RSC Advances 5 (2015) 26017-26026.
[5] J. Li, P. Zhang, X. Zhao, L. Chen, J. Shen, M. Li, B. Ji, L. Song, Y. Wu, D. Liu, Journal of Colloid and Interface Science 549 (2019) 236-245.
[6] S. Sanati, Z. Rezvani, Chemical Engineering Journal 362 (2019) 743-757.
[7] G. Wang, Z. Jin, Journal of Materials Chemistry C 9 (2021) 620-632.
[8] A.A. Lobinsky, V.P. Tolstoy, L.B. Gulina, Applied Surface Science 320 (2014) 609-613.
[9] Y.-W. Long, H.-Y. Zeng, H.-B. Li, K.-M. Zou, S. Xu, X.-J. Cao, Electrochimica Acta 361 (2020) 137098.
[10] Z. Huang, S. Wang, J. Wang, Y. Yu, J. Wen, R. Li, Electrochimica Acta 152 (2015) 117-125.
[11] L. Wang, D. Wang, X.Y. Dong, Z.J. Zhang, X.F. Pei, X.J. Chen, B. Chen, J. Jin, Chemical Communications 47 (2011) 3556-3558.
[12] J. Han, Y. Dou, J. Zhao, M. Wei, D.G. Evans, X. Duan, Small 9 (2013) 98-106.
[13] J. Li, D. Chen, Q. Wu, Journal of Energy Storage 23 (2019) 511-514.
[14] J. Deng, L. Kang, G. Bai, Y. Li, P. Li, X. Liu, Y. Yang, F. Gao, W. Liang, Electrochimica Acta 132 (2014) 127-135.
[15] K. Wang, Q. Li, Z. Ren, C. Li, Y. Chu, Z. Wang, M. Zhang, H. Wu, Q. Zhang, Small 16 (2020) 2001987.
[16] K. Wang, S. Wang, J. Liu, Y. Guo, F. Mao, H. Wu, Q. Zhang, ACS Applied Materials & Interfaces 13 (2021) 15315-15323.